BIOCHEMISTRY
including biophysical chemistry & molecular biology

Article

pubs.acs.org/biochemistry

Mitochondrial ATP Synthase Catalytic Mechanism: A Novel Visual Comparative Structural Approach Emphasizes Pivotal Roles for Mg^{2+} and P-Loop Residues in Making ATP

David J. Blum,[†] Young H. Ko,[‡] and Peter L. Pedersen*,[†]

[†]Department of Biological Chemistry, The Johns Hopkins University, School of Medicine, 725 North Wolfe Street, Baltimore, Maryland 21205-2185, United States

[‡]Cancer Cure Med, LLC, 300 Redland Court, Suite 212, Owings Mills, Maryland 21117, United States

Supporting Information

ABSTRACT: The mitochondrial ATP synthase (F_oF_1) is one of the most abundant, important, and complex enzymes found in animals and humans. In earlier studies, we used the photosensitive phosphate analogue vanadate (V_i) to study the enzyme's mechanism in the transition state. Significantly, these studies showed that Mg^{2+} plays an important role in transition state formation during ATP synthesis. Additionally, in both MgADP·V_i-F_1 and MgV_i-F_1 complexes, photoactivation of orthovanadate (V_i) induced cleavage at the third residue within the P-loop (GGAGVGKT), i.e., βA158, suggesting its proximity to the γ-phosphate during transition state formation. However, despite our recent release of the F_1-ATPase structure containing V_i, the structural details regarding the role of Mg^{2+} have remained elusive. Therefore, in this study, we sought to improve our understanding of the essential role of Mg^{2+} during transition state formation. We utilized Protein Data Bank structural data representing different conformational intermediates of key steps in ATP synthesis to assemble a database of positional relationships between landmark residues of the catalytic site and the bound ligand. Applying novel bioinformatics methods, we combined the resulting interatomic spatial data with an animated model of the catalytic site to visualize the exact nature of the changes in these positional relationships during ATP synthesis. The results of these studies reported here show that the absence of Mg^{2+} results in migration of inorganic phosphate (P_i) from βA158 to a more medial position in the P-loop binding pocket, thereby disrupting essential placement and orientation of the P_i needed to form the transition state structure and therefore MgATP.

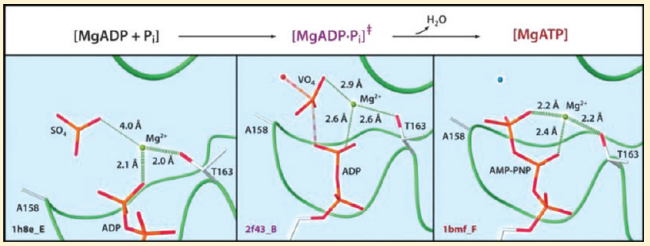

The determination of enzyme structure has always played a prominent role in further elucidating what is known about the functional mechanism of ATP synthase. Early biochemical studies showed that the catalytic F_1 headpiece of the ATP synthase is comprised of five subunit types in an $\alpha_3\beta_3\gamma\delta\varepsilon$ stoichiometric ratio.[1,2] In addition, early EM studies[3] showed the headpiece of F_1 to be comprised of a hexameric arrangement of α and β subunits surrounding a centrally placed subunit complex, now known to be $\gamma\delta\varepsilon$. Numerous studies aimed at deciphering the kinetics and nucleotide occupancy of F_1 made great strides in outlining the overall mechanism.[4−9] With this structural data and other biochemical studies of that and the subsequent decade, it was later proposed and shown that ATP synthesis by F_1 is dependent on "rotary catalysis".[10−12] Thus, the γ subunit was found to rotate within the $\alpha\beta$ hexamer, causing each $\alpha\beta$ pair to change between different conformations in the reaction pathway. As γ rotated under synthesis conditions, each catalytic site within each $\alpha\beta$ pair was perceived to undergo "in turn" a series of conformational changes that "open" the active site to bind ADP and inorganic phosphate (P_i), synthesize ATP from ADP and P_i, and release bound ATP to the surrounding medium via changes in its binding affinity (Figure 1A−C). This has come to be known as the "binding change mechanism".[10]

While the binding change mechanism underscored the overall function of the enzyme in interconverting the electrochemical energy produced by the respiratory chain into chemical energy within ATP, later research[13] aimed to further dissect this broad view into four major levels of mechanism to better investigate discrete steps comprising this elaborate process. Each of these four steps describes a key event in ATP synthesis. The first level of mechanism involves the interconversion of proton motive force into mechanical energy in the form of γ subunit rotation.[14,15] The second level of mechanism involves coupling the γ rotation to binding changes in each of three $\alpha\beta$ pairs that comprise the headpiece of F_1.[16] The third level of mechanism takes place within the active sites located at each $\alpha\beta$ interface (predominately in the β subunit) and consists of the reaction pathway, transition state, and role of the phosphate binding loop (P-loop). The fourth and final

Received: October 17, 2011
Revised: December 10, 2011
Published: December 22, 2011

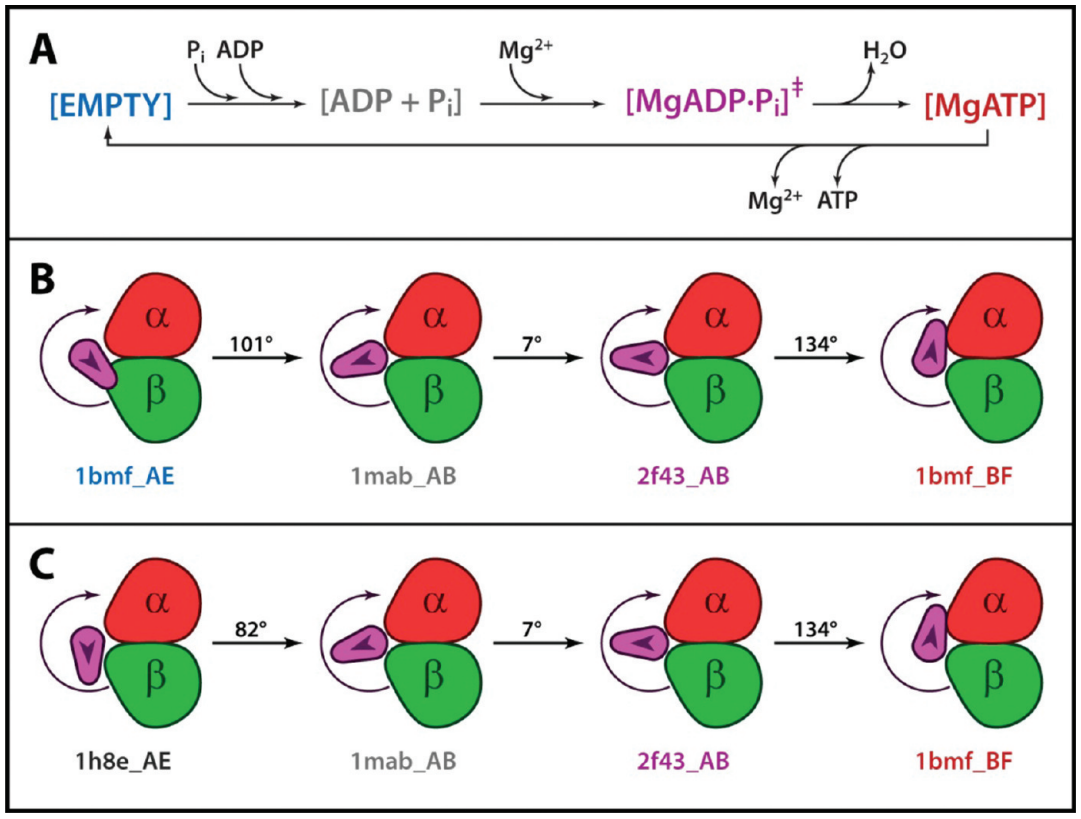

Figure 1. Modeling the reaction coordinate of ATP synthase. (A) This schematic represents key steps in the reaction coordinate of the ATP synthase defined as reaction model 1 in Materials and Methods. In this model, the reaction begins in the empty state and converts into a substrate-bound state following binding of P_i and ADP. Once Mg^{2+} binds, the transition state is formed. Next, water is released, resulting in the product-bound state containing Mg^{2+} and ATP. Upon release of product, the active site returns to the empty state. (B) This conceptual image depicts isolated $\alpha\beta\gamma$ catalytic and rotational units representing each reaction coordinate intermediate as outlined in reaction model 1 (outlined in Materials and Methods). In doing so, this image illustrates the differences in the rotational phase of the γ subunit throughout the reaction. Reaction model 1 utilizes structural data from the following PDB entries: 1bmf_AE,[47] 1mab_AB,[48] 2f43_AB,[29] and 1bmf_BF.[47] The rotational phase was calculated from the aligned structures in Autodesk 3ds Max, using the purported rotational axis and the position of the α-carbon of γR33. Rotation of this atom reference point results in changes to the x and y coordinates, with almost no change in the z axis. (C) This conceptual image depicts isolated $\alpha\beta\gamma$ catalytic and rotational units representing each reaction coordinate intermediate as outlined in reaction model 2 (outlined in Materials and Methods). In doing so, this image illustrates the differences in the rotational phase of the γ subunit throughout the reaction. Reaction model 2 utilizes structural data from the following PDB entries: 1h8e_AE,[49] 1mab_AB,[48] 2f43_AB,[29] and 1bmf_BF.[47] The rotational phase was calculated from the aligned structures in Autodesk 3ds Max, using the purported rotational axis and the position of the α-carbon of γR33. Rotation of this atom reference point results in changes to the x and y coordinates, with almost no change in the z axis.

step in the process independent of the actual mechanism of ATP synthesis per se is the release of the bound ATP.

Via closer examination of the third level of mechanism at the active site, the past two decades have provided vast amounts of experimental data describing the biochemical and structural attributes of F_1, with much of the attention focused on the various aspects of the P-loop. The P-loop is a glycine rich region that is highly conserved (GXXXXGKT/S) from bacteria to humans and is found in numerous nucleotide binding proteins.[17,18] This structural motif exhibits a C-shaped density that wraps around the interface among ADP, P_i, and Mg^{2+} helping to form the catalytic pocket (Figure 2A–D). This arrangement places several key residues circumferentially about the reaction center of the catalytic site,[19] with βA158 and βT163 being the terminal residues of this clamplike domain. While mutagenesis studies[20−28] have established the individual significance of several P-loop amino acids, the nature of their concerted contribution to the synthesis of ATP has remained unclear.

During this pivotal era (1998−2011), 20 crystal structures have been determined for mitochondrial F_1-ATPase, including 56 unique conformers of the catalytic site for ATP synthesis. In recent years, one of the most significant has been the transition state structure determined for the F_1-ATPase from rat liver mitochondria in the presence of ADP, Mg^{2+}, and orthovanadate (V_i), a transition state phosphate analogue.[29] This crystallographic study was crucial to further describe the reaction pathway occurring at the catalytic site. When presented, it confirmed structural details of the trigonal bipyramidal ligand geometry that were expected in a transition state as shown by landmark studies on myosin ATPase.[30,31]

While these crystallographic data were indispensable in the elucidation of a more complete view of the concerted role of P-loop residues in catalysis, earlier biochemical studies with V_i had emphasized the important role of βA158 and Mg^{2+} in transition state formation. Initial studies utilizing the phosphate analogue, V_i, in the presence of ultraviolet (UV) light and O_2 demonstrated peptide bond cleavage at the third position within the nucleotide binding consensus (GGAGVGKT), i.e., at βA158 in a single β subunit per molecule of F_1.[32] This study showed that the third position of the P-loop was within contact distance of the γ-phosphate during the transition state as seen

dx.doi.org/10.1021/bi201595v | Biochemistry 2012, 51, 1532−1546

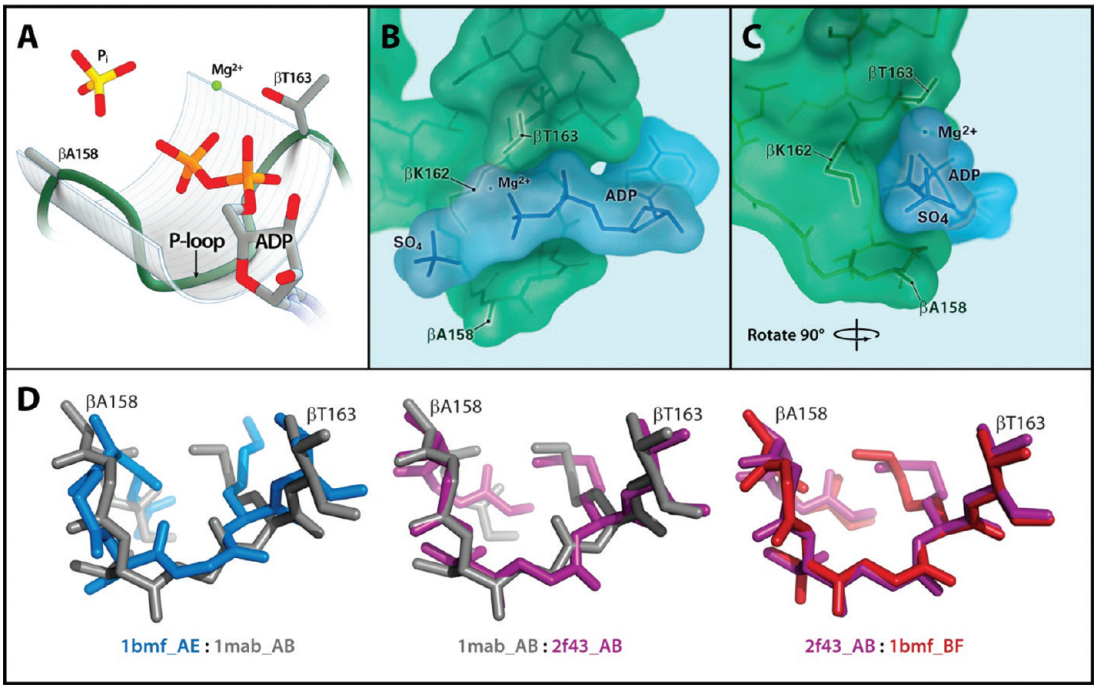

Figure 2. Structure of the P-loop clamp in the β subunit of F_1 within the ATP synthase. (A) This conceptual image illustrates the P-loop clamp. The third (βA158) and eighth (βT163) residues are represented in stick form at either end of this clamplike structure that surrounds ADP, P_i, and Mg^{2+}. (B) By viewing a fragment of the β subunit (green) containing the P-loop clamp from an angle that is roughly perpendicular to the substrate (blue), we are able to appreciate the inline placement of both βA158 and βT163 at the interface among ADP, P_i, and Mg^{2+}. (C) With rotation of panel B 90° along the vertical axis, it becomes possible to see that the P-loop clamp wraps circumferentially around the reaction center. These models were based on structural data from PDB entry 1h8e. (D) This illustration depicts the pairwise structural alignments of adjacent conformational intermediates of the P-loop in reaction model 1. The first set of superimposed structures is between the empty state (PDB entry 1bmf_E, blue) and the substrate-bound state containing ADP and P_i (PDB entry 1mab_B, gray). The second set of superimposed structures is between the substrate-bound state (PDB entry 1mab_B, gray) and the transition state analogue (PDB entry 2f43_B, magenta). The final set of superimposed structures is between the transition state analogue (PDB entry 2f43_B, magenta) and the product-bound state containing Mg^{2+} and ATP (PDB entry 1bmf_F, red).

in comparable studies with myosin[30] and adenylate kinase,[33] although each enzyme contained a different resident amino acid at that position. This was later confirmed by X-ray crystallographic studies.[29,34] An additional study[35] using V_i to trap F_1 in a transition state-like complex discovered that while Mg^{2+}, ADP, and V_i significantly inhibited the ATPase activity via formation of a MgADP·V_i-F_1 complex, the MgV_i-F_1 complex was inhibited to nearly the same extent. However, in the absence of Mg^{2+}, the ATPase activity of both the V_i-F_1 and ADP·V_i-F_1 complexes exhibited almost no inhibition as seen in the F_1 control. This novel finding clearly demonstrated the importance of Mg^{2+} in transition state formation, although the exact mechanism remained unclear.

Additional studies utilizing an active site tryptophan mutant (βY331W) as a fluorescent probe in the ATP synthase of *Escherichia coli* were used to explore the relationship between nucleotide binding and occupancy with ATP hydrolysis under equilibrium conditions.[36] In this study, Löbau et al.[36] demonstrated that P_i does not spontaneously bind without the input of energy from γ subunit rotation and the proton gradient that drives rotation during ATP synthesis, suggesting that radical remodeling of the P_i binding pocket is required to modulate binding affinity. These findings led to further fluorescence and mutagenesis studies for characterizing the P_i binding pocket.[37−44] The studies identified several key residues, including two P-loop side chains involved in P_i binding and transition state stabilization. In addition, these studies highlighted the role of αR373, βN243, βR246, βR182, βK155, and βT156 (in *E. coli*) in the proper placement, orientation, and transition state stabilization of P_i within the active site during catalysis.[36−43,45] The importance of this network of interactions is underscored in the work of Senior et al.[46] that revealed that ADP, Mg^{2+}, and P_i require firm anchoring and exquisite orientation within the active site to overcome charge repulsion as ADP and P_i are thrust together.

In the case of exploring enzyme function, enzyme structure is used consistently to elucidate potential details of enzyme mechanism. In the novel bioinformatic approach described here, we used available PDB structures for F_1,[29,47−49] two of which are of rat liver F_1[29,48] purified earlier in the authors' laboratory.[2] Positional relationships between pertinent P-loop residues of the β subunit catalytic site and its bound ligand were measured and collected into a centralized database representing the different conformational intermediates of the reaction coordinate. Additionally, a visual three-dimensional (3D) model of the reaction pathway was created using Cartesian data points retrieved from the PDB files. This allowed the database of positional changes to be compared directly with specific conformational changes seen in the visual model to improve our understanding of the role of these interatomic relationships in the mechanism of ATP synthesis.

Significantly, the studies described here provide novel insight into the reaction pathway involved in ATP synthesis via the catalytic F_1-ATPase headpiece. Moreover, they support the view that in the presence of Mg^{2+}, P_i moves into the phosphate binding pocket near βA158, thereby facilitating formation of the transition state. In addition, this study emphasizes a pivotal and essential role of Mg^{2+} together with the P-loop residues,

dx.doi.org/10.1021/bi201595v | *Biochemistry* 2012, 51, 1532−1546

βA158 and βT163, in the formation of the transition state during ATP synthesis.

MATERIALS AND METHODS

Selection and Retrieval of Data Sets. The Protein Data Bank, blastp,[50] and the National Center for Biotechnology Information (NCBI) were used to search for all available structures of mitochondrial F_1-ATPase. The results were filtered to exclude nonsubstrate inhibitors like I1-60his,[51] quercetin,[52] resveratrol,[52] and azide[53] as these structures are more valuable for determining the mechanism of inhibition of the given chemical agent, as opposed to elucidating the mechanism of ATP synthesis at the active site. To provide the highest-quality data for this study, the results were filtered to exclude low-resolution structures like those containing subunits in addition to the catalytic F_1 moiety[54] or those studying humidity control.[55] The primary objective was to attain those structures that best represent key intermediates in the reaction mechanism outlined in Figure 1A.

After close inspection of the ligand-bound state of the available PDB models, only four PDB files were identified that best represented the potential conformational intermediates of the reaction pathway of ATP synthesis (Table S1 of the Supporting Information). These PDB files (1bmf, 1mab, 1h8e, and 2f43) were downloaded from the RCSB Protein Data Bank[56] in the protein data bank (PDB) file format (http://www.rcsb.org). Discovery Studio 2.0, DeepView Swiss-PdbViewer,[57] and Pymol[58] were used to view and carefully analyze the different protein structures.

Analysis of Conformational Differences. Swiss-PdbViewer was used to perform pairwise structural alignments to assess conformational differences between the subunits, domains, and subdomains of dissimilar catalytic αβ pairs of the reported PDB structures. Alignments were performed using equivalent selection groups and were fitted according to the α-carbons of the peptide backbone. Following each cycle of selection and alignment, a pairwise root-mean-square deviation (rmsd) was calculated to evaluate conformational differences in the region or subunit of interest. All rmsds were reported in angstroms.

Surveying Positional Differences between Catalytic Sites of Different Conformational States. Interatomic distances between landmark atoms of both key residues and bound ligand were calculated using Discovery Studio and Pymol. These distances were recorded into a database and organized to create a three-dimensional map of the active site in each of the intermediate states. Atom-to-atom distances reported for each catalytic αβ pair were derived from the original PDB structure retrieved from the RCSB PDB. All distances are reported in angstroms. The *B* factor for each of the β subunits was normalized to assess, and compare, the structural flexibility of the system being studied.[59] The *B* factors were normalized to zero mean and unit variance using the following equation:

$$B^{N} = (B - B^{\mu})/B^{\sigma}$$

where B^N is the normalized *B* factor, *B* is the actual *B* factor, B^{μ} is the average *B* factor, and B^{σ} is the standard deviation for all atoms in each PDB entry. All normalized *B* factors are reported in square angstroms.

Alignment of Catalytic αβ Pairs with a Common Coordinate System To Allow Simulation of Geometric Changes Associated with Rotation of the γ Subunit. To visualize conformational differences between dissimilar subunits, two or more structures are aligned with a defined and mutual three-dimensional space. To achieve a best fit, a selected group of equivalent residues is typically aligned by α-carbon positions. However, because ATP is synthesized via rotary catalysis by F_1, a novel method of alignment was employed to reveal conformational differences as a function of γ subunit rotation. Analysis of differences in tertiary structure revealed that the N-terminal domains exhibit consistently lower rmsds with less variation than that of the nucleotide binding and C-terminal domains. These values suggest that, as a result of γ subunit rotation, this region does not undergo significant subdomain conformational changes like that of the nucleotide binding and C-terminal domains of the β subunit. Averaged 3D coordinates of residues α24−90 and β9−81 revealed that the N-terminal domain of each catalytic αβ pair is roughly equidistant from a common central axis with placement nearly 120° apart denoting a rotational symmetry. The consistency of these structural traits of the N-terminal domain under greatly varied catalytic conditions suggests that the conformational state at both the tertiary and quaternary level is stable and minimally active during γ subunit rotation. Therefore, conformational intermediates of each αβ pair were aligned by an array of coordinates representing the averaged N-terminal domain coordinates of each of three catalytic αβ pairs present in the biological unit of their respective PDB files. This resulted in an alignment of each catalytic unit along the inferred rotational axis, allowing for analysis of the conformational differences that result from γ subunit rotation.

To set up the rotational axis guide, averages of the three-dimensional coordinates of all atoms from the N-terminal regions of both the α and β subunit (residues α24−90 and β9−81, respectively) were calculated for each αβ pair. The three resultant points were averaged to define the central axis in relation to the three catalytic αβ pairs. Nine additional points were then projected along a vector perpendicular to the plane defined by the original three averages at 20 Å intervals (Figure 3). This arrangement of 13 points was appended to the PDB file from which it was derived. This process was repeated for the remaining PDB structures. To ensure its use as an alignment tool in Swiss-PdbViewer, each three-dimensional coordinate was added to the PDB file as an ATOM record. The three active sites were named GOL620, GOL621, and GOL622, with the 10 coordinates of the rotational axis named GOL623−632. These coordinates were defined as chainID "K" to aid in selection and use in alignment. Each PDB file was duplicated to create three copies of each structure with the embedded orientation markers. The names of embedded markers for GOL620−622 were changed such that GOL620 designated the αβ pair of interest and the files were named (PDB ID_CHAIN ID) accordingly, i.e., 1bmf_AE, 1bmf_BF, 1h8e_AE, 1mab_AB, and 2f43_AB. Via orientation of the rotational axis guide to a specific αβ pair, all conformational intermediates could be aligned to a common coordinate system; i.e., they all overlap at one position.

Calculation of the Rotational Phase of the γ Subunit To Determine Reaction Sequence. To verify the reaction sequence of the available structures based on ligand binding, the rotational phase of the γ subunit was measured for each catalytic unit using Autodesk 3ds Max. The alignment guide described above (consisting of GOL620−632) was created in 3ds Max using simple spheres. Upon careful examination of the

dx.doi.org/10.1021/bi201595v | Biochemistry 2012, 51, 1532−1546

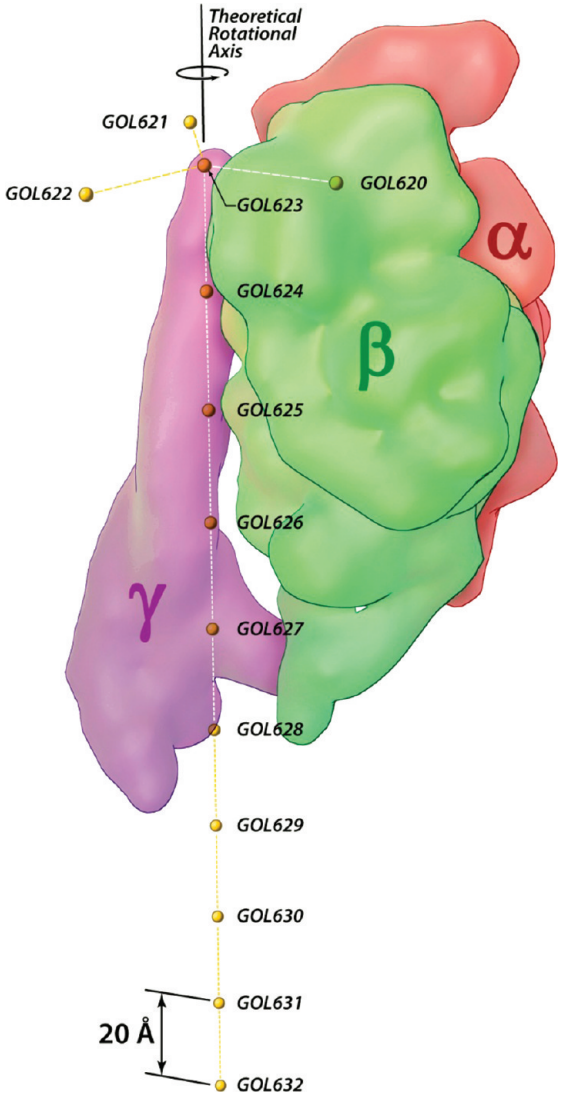

Figure 3. Creation of a rotational axis guide used in alignment of the $\alpha\beta\gamma$ asymmetric unit. This conceptual image depicts an isolated $\alpha\beta\gamma$ catalytic unit representing one step in the reaction coordinate. The N-terminal regions of an α subunit (residues 24−90) and β subunit (residues 9−81) of a catalytic unit ($\alpha\beta$) were averaged, and ATOM entries for GOL620−622 were placed in these three locations (F_1 has three $\alpha\beta$ catalytic units). ATOM entry GOL623 represents an average for the Cartesian coordinates of GOL620−622. ATOM entry GOL620 was placed at the catalytic unit of interest. Nine additional ATOM entries were placed 20 Å apart, perpendicular to the triangular plane formed by GOL620−622. This line of atoms represents the theoretical rotational axis, as described in Materials and Methods. This process was performed on each catalytic unit, and the resulting axial structure was used to align all catalytic units with a common 3D space along the proposed rotational axis of the γ subunit. This model was based on structural data from PDB entry 1mab.

γ subunit of the selected PDB files, it was determined that the α-carbon of γR33 best represented the asymmetric orientation of γ in relation to its rotational axis. Theoretical rotation of this atom reference point around the rotational axis results in changes to the x and y coordinates, with almost no change in the z axis. This atom reference point was created in 3ds Max for each of the catalytic units. Using the rotational axis as the center, the angle between adjacent intermediates was calculated from the empty state to the product-bound state (Figure 1B,C). This methodology was used to confirm the proposed order of available PDB structures.

Design and Construction of Kinematic Skeleton, Hierarchical Controls, and 3D Models. Recently, the advancement of 3D tools used in computer animation has been driven extensively by cinematic needs. Autodesk 3ds Max is one of the most advanced 3D modeling and animation tools available today and was used to create all 3D assets used in this study. Use of a kinematic skeleton allows translational and rotational data input to be transferred in a hierarchical fashion downstream from the parent object to children in a linear and iterative fashion. The kinematic skeleton was constructed of basic parametric nonrenderable objects, each of which represents a skeletal bone that can be virtually modified or monitored.

Construction of the kinematic skeleton was based on the MgATP-bound state of the enzyme as a common conformational intermediate of the reaction pathway to be modeled. The hierarchies for the peptide backbone atoms were created first. A spherical bone was created at the orthogonal coordinates of each backbone atom from βD141 to βG204 for the structural intermediate of 1bmf_BF. Skeletal elements were also created for side chain atoms of βA158, βT163, and βE188, as well as bound ligand present throughout the reaction pathway. Two cylindrical bones were created along every bond with the exception of those that led to terminal atoms. The first cylindrical bone was used to establish bond alignment between different states, and the other was used to modify the torsional angle of the bond at that location. They were named "alignment guide" and "rotational guide", respectively. The hierarchy was set up to allow transitional and rotational control of the bones that maintain bond lengths and angles during the transition from state to state throughout the reaction coordinate. These changes are in turn translated to downstream child objects.

Starting from βG204, we applied the pattern of hierarchy such that in each peptide unit the carbon of the carboxyl group was parented to the rotational guide just N-terminal of the associated α-carbon. This rotational guide was parented to the alignment guide at the same orthogonal coordinates, which was in turn parented to the aforementioned α-carbon. This α-carbon was then parented to the rotational guide just N-terminal of the associated nitrogen of the amino group. This cycle of inheritance was repeated until all atoms of the peptide backbone had been linked from βG204 to βD141 through the rotational and alignment guides of each bond of the backbone. This construct makes the N-terminal nitrogen of βD141 the overall parent for the entire kinematic skeleton.

Side chain bones utilize an identical pattern of hierarchy, starting at the terminal and branching atoms and proceeding to the α-carbon of each residue. To make the transition from one state to the next, translational changes were keyed in starting at the N-terminus and proceeding to the C-terminus. After a given atom was "moved", i.e., from its initial coordinate to the next along the reaction pathway, the alignment guide was in turn aligned with the next associated alignment marker for the new intermediate state. This in turn aligned the rotational guide with the new vector. Once aligned, the rotational guide was rotated to best fit the next level atoms to the new positional coordinates. Once these atoms were aligned with the new set of coordinates, the process was repeated until the C-terminal βG204 residue was reached.

dx.doi.org/10.1021/bi201595v | *Biochemistry* 2012, 51, 1532−1546

All models were created in Autodesk 3ds Max using basic parametric objects and editable splines. Each object was created at the orthogonal coordinates defined by the PDB files. These models were parented to a kinematic skeleton that allows hierarchical control of the translational and rotational properties along the peptide chain and side chain atoms.

Modeling Comparisons To Elucidate the Role of Positional Change in the Reaction Coordinate. The ATP synthase has three nucleotide binding sites ("active sites") that catalyze ATP synthesis. Each active site proceeds through the following reaction pathway as the γ subunit rotates 360°: empty, Mg·ADP- and P_i-bound, transition state, Mg·ATP-bound, and the empty state. The "E" chain of PDB entry 1bmf[47] was chosen to represent the empty state and has no ligand bound. Only two of the available PDB files contained an $\alpha\beta$ catalytic unit with ADP and P_i bound; however, only one of these structures contained Mg^{2+} in the active site, and the other represents an early state in substrate binding. While neither structure represents an ideal MgADP- and P_i-bound state, both structures could offer significant insight into the presynthesis substrate-bound state. The "B" chain of PDB entry 2f43[29] was chosen as the best representation of the transition state analogue because of previous active site comparisons[29] among proposed transition state analogue structures 1e1r,[60] 1h8e,[49] and 2f43.[29] Lastly, the "F" chain of PDB entry 1bmf[47] was chosen to represent the product-bound state containing MgAMP-PNP, a nonhydrolyzable analogue of ATP. With these structures, two models of the reaction coordinate were designed on the basis of available structural data. Reaction model 1 ($A^1 \rightarrow B \rightarrow C$) represents a pathway starting with an ADP- and P_i-bound ground state (1mab_AB), followed by the transition state-like conformation with Mg^{2+}, ADP, and V_i bound (2f43_AB), and finally the ground state with Mg^{2+} and AMP-PNP (nonhydrolyzable ATP analogue) bound (1bmf_BF). The first model serves to visualize the structural changes that occur in the transition from the absence of Mg^{2+} to the presence of Mg^{2+} and the formation of the transition state.

Preliminary mapping of the active site using rmsd calculations of each catalytic $\alpha\beta$ pair demonstrated that the "half-closed" (HC) conformation (1h8e_AE) of the catalytic $\alpha\beta$ pair offered insight into the early status of phosphate binding in the reaction coordinate and was the only premature reaction structure currently available with Mg^{2+}, ADP, and SO_4 (P_i analogue) bound.[49] Therefore, reaction model 2 ($A^2 \rightarrow B \rightarrow C$) represents an early Mg^{2+}-, ADP-, and P_i-bound ground state (1h8e_AE), followed by the transition state analog, and the Mg^{2+}·AMP-PNP-bound state of the first model. This model is used to visualize positional changes among βA158, βT163, and βE188 as well as the relationship these residues have with Mg^{2+}, ADP and ATP, and P_i from very early in the reaction coordinate to product formation. The value of this novel modeling technique is that it can be applied in the future to the study of other enzymes having the requisite intermediate structural data.

RESULTS AND DISCUSSION

N-Terminal Domains of α and β Subunits Undergo Minimal Conformational Change, while Both the Nucleotide Binding and C-Terminal Domains of the β Subunit Undergo More Significant Conformational Changes Associated with Their Transition through the Reaction Pathway. As outlined by the binding change mechanism, each of the three catalytic $\alpha\beta$ pairs that comprise F_1's transition through a series of conformational intermediates does so in the presence of Mg^{2+} as a direct response to γ subunit rotation to produce MgATP from MgADP and inorganic phosphate. Among available X-ray crystallographic data for F_1-ATPases, five structures were used here; these included four structures that contained catalytic $\alpha\beta$ pairs representing an empty state (1bmf_AE), a substrate-bound state containing ADP and P_i (1mab_AB), a transition state analogue containing bound MgADP·V_i (2f43_AB), and a product-bound state containing MgAMP-PNP (1bmf_BF). In the fifth structure (1h8e_AE), an $\alpha\beta$ pair was utilized because of its unique conformational character and bound ligand (MgADP and SO_4). To better understand the changes that occur in tertiary and quaternary structure as a function of γ subunit rotation using these PDB structures, pairwise rmsds were calculated for comparable selection groups between individual $\alpha\beta$ pairs, α and β subunits only, and structural motifs of α and β subunits. These results are presented in Table S2 of the Supporting Information.

Pairwise rmsds between $\alpha\beta$ pairs, stepwise from the empty state to the product-bound state, revealed that the greatest conformational difference was present in alignment of the empty state with that of the ADP- and P_i-bound state at 4.64 Å for 935 backbone atoms (C_α only). Subsequent pairwise rmsd calculations for individual α and β subunits for these intermediates demonstrated that the greatest conformational difference was present in an alignment of the empty state with that of the ADP- and P_i-bound state, at 3.98 Å for 456 backbone atoms (C_α only) from the β subunit and significantly less for the α subunit at 1.32 Å for 479 backbone atoms (C_α only). Further investigation of the N-terminal, nucleotide binding, and C-terminal domains of both the α and β subunits of these intermediates revealed that the greatest conformational difference (rmsd) was located predominately within both the nucleotide binding domains (NBDs) and the C-terminal domains of the β subunit at 2.95 Å for 282 backbone atoms (C_α only) and 2.33 Å for 101 backbone atoms (C_α only), respectively.

For structural alignments between the transition state analogue and the product-bound state, more moderate conformational differences (rmsd) between $\alpha\beta$ pairs were observed at 1.61 Å for 935 backbone atoms (C_α only). Further analysis of structural alignments between individual α and β subunits showed conformational differences (rmsd) at 1.38 Å for 479 backbone atoms (C_α only) and 1.18 Å for 456 backbone atoms (C_α only), respectively. Looking closer at alignments for the three domains of both α and β subunits illustrated that the greatest conformational differences (rmsd) occurred in the C-terminal domains of both α and β subunits with rmsds of 1.81 Å for 123 backbone atoms (C_α only) and 2.16 Å for 101 backbone atoms (C_α only), respectively. Structural alignments of the P-loop of the β subunit showed that there were no significant differences between these intermediates with an rmsd of 0.39 Å for eight backbone atoms (C_α only). However, there was a moderate opening of the P-loop with the transition from the empty to the substrate-bound state (Figure 2D).

Additional investigation using structural alignments was performed between reaction coordinate intermediates and that of the A and E chains from 1h8e. This particular $\alpha\beta$ pair from 1h8e contains bound MgADP and SO_4 and appears to represent an early state in synthesis, i.e., when the active site is

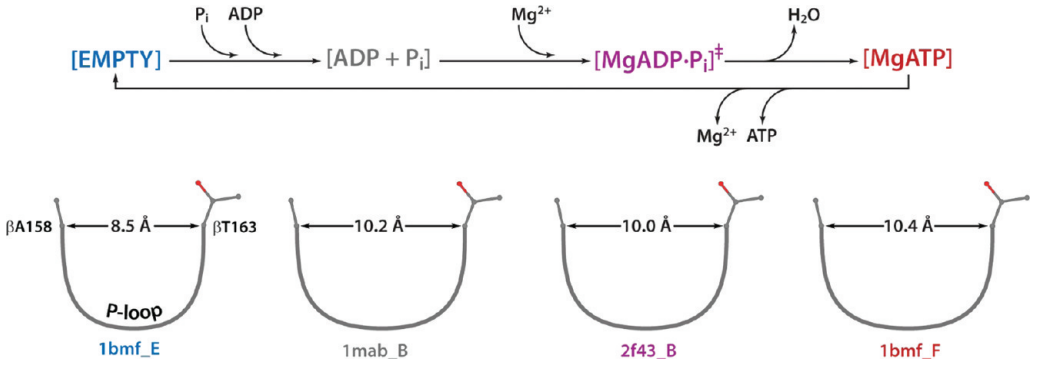

Figure 4. Positional dynamics within the P-loop clamp in the catalytic site of ATP synthase. This schematic diagram illustrates changes in the interatomic distances of the β subunit P-loop clamp at the α-carbons of βA158 and βT163 throughout the reaction coordinate. All distances are reported in angstroms.

still mostly open. Results from these structural alignments showed that the MgADP- and SO_4-bound state was actually closest in conformation to the empty state at nearly all previously mentioned levels of alignment, significantly more so than any other intermediate from the reaction coordinate used in this study. However, despite this close conformational nature, its P-loop conformation in the β subunit was closest to the product-bound state and transition state analogue with rmsds of 0.30 and 0.53 Å for eight backbone atoms (C_α only), respectively, as opposed to that of the empty state with an rmsd of 1.39 Å for the same selection group. The complete results are listed in Table S3 of the Supporting Information.

Overall, for all structural alignments performed among the three $\alpha\beta$ pairs mentioned above, a minimal conformational difference was observed for N-terminal domains on both α and β subunits, with rmsd values ranging from 0.23 to 0.66 Å. These data suggest that the N-terminal domain undergoes a minimal conformational change as a function of γ subunit rotation. The more significant conformational differences occur in the nucleotide binding and C-terminal domains of both α and β subunits, albeit predominately in β.

P-Loop residues, βA158 and βT163, Undergo Minimal Change (<0.5 Å) at the Level of Backbone and Terminal Atom Distances As Demonstrated by Conformational Intermediates Representing Key Steps in the Reaction Coordinate. In a previous report, Ko et al.[32] demonstrated that the F_1 moiety of the ATP synthase is significantly inhibited by V_i, a phosphate analogue that induces a transition state-like structure in ATP synthase. When the MgADP·V_i-F_1 complex was exposed to O_2 and UV light, βA158 was found to be the site of peptide bond cleavage in a single β subunit, suggesting that this residue moved closer to the γ-phosphate of ATP during catalysis.

To begin to characterize changes in the positional relationship between βA158 and the would be γ-phosphate during catalysis, we first recorded the interatomic distance between the α-carbons and terminal side chain atoms (-CH_3 and -OH) of βA158 and βT163 as well as α-carbon distances between both βA158 and βK162 throughout the prescribed conformational intermediates. These dimensions are important because βA158 and βT163 are on opposite sides of the P-loop. Here, they form part of the catalytic pocket. If βA158 moves more into the catalytic pocket, and thus closer to the γ-phosphate, we would expect these dimensions to decrease when the transition state is formed. The results are recorded in Table S4 of the Supporting Information.

In the empty state, the α-carbons of βA158 and βT163 are 8.5 Å apart, which is the most "closed" state seen in the P-loop clamp of the five conformational intermediates measured. Upon binding ADP and P_i, as seen in 1mab_B, the P-loop clamp opens by 1.7 Å, with a 0.5 Å opening at the terminal side chain atoms (-CH_3 and -OH) (Figure 4 and Animation S1 of the Supporting Information). When Mg^{2+} binds to the active site, followed by formation of the transition state, the α-carbons of βA158 and βT163 move closer by 0.2 Å, while the terminal atoms of the same residues actually separate by 0.4 Å. Upon formation of ATP, the interatomic distances between the terminal atoms remain virtually unchanged, while the distance between the α-carbons increases by 0.4 Å.

While a slight opening and closing of the P-loop is observed through the reaction coordinate, these positional relationships do not account for the dramatic difference needed to place βA158 nearly 1.4 Å closer to the γ-phosphate. The empty state, on the other hand, represents the most closed state of the P-loop. These findings suggest that the P-loop clamp is closed tightest in the absence of bound ligand and opens to allow binding of substrate to synthesize product.

βE188 Is Closest to P-Loop Residue βA158 in the Absence of Mg^{2+}, Almost Identical to That of the Transition State Structure. The positional relationship between βA158 and βE188 defines a second clamplike interface surrounding P_i, but oriented nearly 50° from the axis of the P-loop clamp (Figure 5). To understand the importance of their spatial relationship and how it changes during catalysis, we calculated the interatomic distances between both backbone and terminal side chain atoms (-CH_3 and -OE_x) of βA158 and βE188. The results are listed in Table S5 of the Supporting Information.

In the empty state, βE188 is nearly 12 Å from βA158 based on the interatomic dimensions at the terminal side chain atoms (Figure 6A and Animation S2 of the Supporting Information). However, once ADP and P_i are bound, this distance is reduced by 4.4 Å and is nearly identical to that of the transition state analogue. In fact, the Mg^{2+} free state seen in 1mab_AB displays a geometry between βE188 and βA158 nearly identical to that of the transition state analogue. Upon formation of ATP, the distance between βE188 and βA158 increases slightly. These findings support the purported role of βE188 in participating in extraction of a water molecule from ADP and P_i during the synthesis of ATP.[13]

In the Absence of Mg^{2+}, P_i Shifts to a More Medial Position in the P-Loop Away from βA158 and Closer to

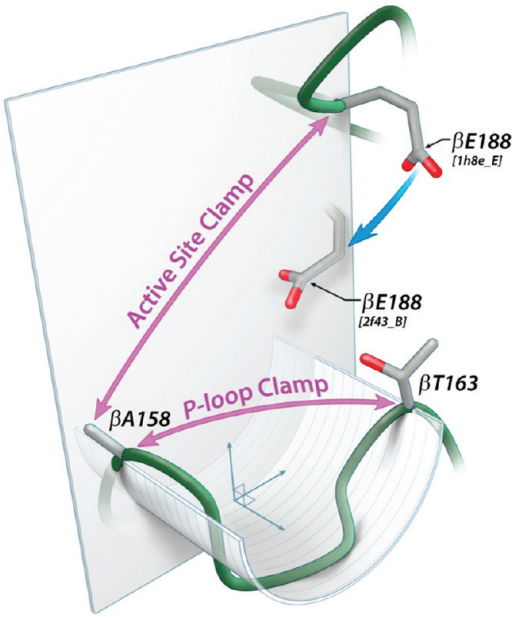

Figure 5. Concept of two clamps within the active site of F_1-ATPase. This conceptual image depicts the active site of a single catalytic active site in the β subunit. In this study, it was determined that there were two separate clamping mechanisms around the reaction center. The first is located within a small domain that forms part of the phosphate binding pocket called the P-loop. The boundaries of the P-loop clamp are demarked by P-loop residues, βA158 and βT163. The second clamp is located within two different subdomains of the nucleotide binding domain in which the active site resides. The boundaries of the active site clamp are defined by βA158 and βE188. This model was based on structural data from PDB entries 1h8e and 2f43.

βT163. In an effort to further characterize the changes occurring in the catalytic site during synthesis, we calculated the interatomic distance between the α-carbons and terminal side chain atoms (-CH$_3$ and -OH) of βA158 and βT163 and that of the would be γ-phosphate for those $\alpha\beta$ pairs representing the reaction coordinate having bound ligand. This distance is essential for determining the center of mass for the would be γ-phosphate within the binding pocket and how this position changes both during catalysis and as a result of changes in occupancy. These data are recorded in Table S6 of the Supporting Information.

When ADP and P_i are bound to the active site as is the case with 1mab_AB, we found the central mass of P_i to be 6.2 Å from the β-carbon of βA158. However, once Mg^{2+} is bound and the transition state is formed, the center of mass for P_i is nearly 1.5 Å closer to the aforementioned β-carbon (Figure 6B and Animation S3 of the Supporting Information). This interatomic distance is nearly identical once ATP has formed in the final product-bound state. Additionally, in the case of the half-closed state (1h8e_AE), we observed that the sulfur atom of sulfate (P_i analogue) was in a nearly identical position relative to the β-carbon of βA158 as found in the transition state-like structure. This might suggest that P-loop geometry is established early, by first binding P_i followed by MgADP as supported by the work of Ko et al.[35] and Watanabe et al.[61] in F-type ATP synthase, and Manimekalai et al.[62] in A-type ATP synthase.

In the presence of Mg^{2+}, the center of mass for P_i maintains a consistent positional relationship with the side chain of βA158, even when the active site is open as seen in the half-closed state. However, in the absence of Mg^{2+}, as seen in the $\alpha\beta$ pair from 1mab_AB, P_i assumes a more central position within the binding pocket, away from βA158, and significantly closer to βT163. These findings, in conjunction with findings associated with the MgV_i-F_1 complex from previous work,[35] suggest that Mg^{2+} is essential for the proper positioning of the γ-phosphate within the P-loop clamping mechanism.

During Formation of the Transition State, P_i Moves into the Proximity of the Methyl Group of the P-Loop Alanine, Aiding in the Removal of Water from the Active Site Formed during the Synthesis of ATP. Earlier results from this study have demonstrated that Mg^{2+} helps to correctly position P_i within the binding pocket and that the center of mass of the phosphorus atom appears to maintain an equivalent interatomic distance with the β-carbon of βA158 throughout the reaction coordinate. To better understand the significance of this positional relationship, we calculated the interatomic distances between the β-carbon of βA158 and that of all four oxygen atoms of P_i throughout the reaction coordinate. These data are recorded in Table S7 of the Supporting Information. (See Table S8 of the Supporting Information for conversion of model nomenclature to actual PDB nomenclature.)

In the ADP- and P_i-bound state, all oxygen atoms of P_i are at least 6.0 Å from the β-carbon of βA158 as it resides medially in the P-loop clamp. However, in the transition state analogue, the oxygen atom closest (3.8 Å) to the hydrophobic methyl group of the P-loop alanine relative to remaining oxygen atoms appears to be an excellent candidate for formation of the leaving group water (Figure 7A and Animation S4 of the Supporting Information). In the ATP-bound state, electron density representing what is thought to be a water molecule near the periphery of the active site, 6.4 Å from the β-carbon of βA158, is positioned as would be expected for water leaving the active site. These data suggest a scenario whereby Mg^{2+} not only ensures placement of P_i near βA158 but also helps steer P_i into the correct orientation necessary for catalysis through its interactions.

The β-Phosphate Oxygen of ADP Is Placed in Line with P_i, Allowing It To Conduct a Nucleophilic Attack on the Phosphorus Atom, Resulting in the Formation of ATP. The synthesis of ATP involves placement of ADP's β-phosphate oxygen, the one with the greatest negative charge, in line with the phosphorus atom of P_i, allowing the oxygen to conduct a nucleophilic attack on the phosphorus atom, resulting in the formation of the MgATP-F_1 complex and a water molecule that readily leaves the active site. To better corroborate the thought that the active site geometry of the selected conformational states is directly involved in the mechanism of ATP synthesis, we calculated the interatomic distances between the atom representative of the phosphorus atom (in the P_i analogues and γ-phosphate of the ATP analogue) and that of the closest oxygen atom of the β-phosphate of ADP and/or ATP throughout the reaction coordinate. These data are recorded in Table S9 of the Supporting Information. (See Table S8 of the Supporting Information for conversion of model nomenclature to actual PDB nomenclature.)

In the half-closed state, representing an early conformational state in the reaction coordinate, the sulfur atom representing the phosphorus atom in the P_i analogue is farthest from the nearest β-phosphate oxygen (4.5 Å). In the transition state analogue, the vanadium atom is now 1.5 Å closer to the nearest β-phosphate oxygen in a trigonal bipyramidal coordination. In

dx.doi.org/10.1021/bi201595v | Biochemistry 2012, 51, 1532–1546

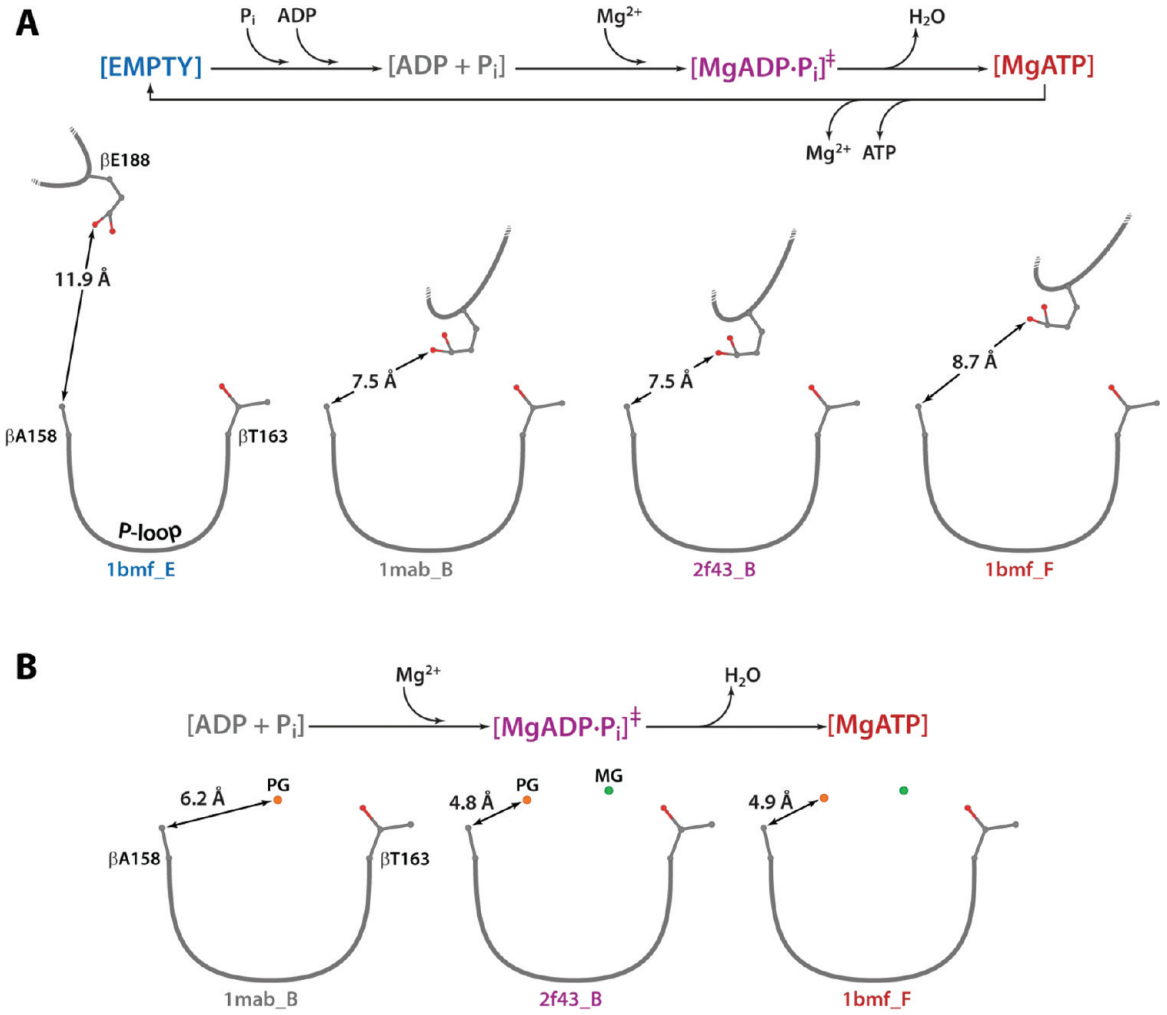

Figure 6. Positional dynamics within the active site clamp in the catalytic site of ATP synthase. (A) This schematic diagram illustrates changes in the interatomic distances of the β subunit active site clamp at the α-carbons of βE188 and βA158 throughout the reaction coordinate. (B) This schematic diagram illustrates positional changes of the γ-phosphate throughout the reaction coordinate by measuring the interatomic distances between the β-carbon of βA158 and the (γ) phosphorus atom. All distances are reported in angstroms.

the final product-bound state, the interatomic distance between the closest oxygen atom of the β-phosphate and the γ-phosphorus atom of ATP is 1.6 Å, which is what is expected for a P−O bond (Figure 7B). The progression in this interatomic distance throughout this model-based reaction coordinate matches what is expected of the relationship between these molecules during the synthesis of ATP.[37,46,63]

The Oxygen from V_i That Is Closest to the Methyl Group of βA158 during the Transition State Is Also Positioned near βE188, Which Is Necessary To Aid in the Formation of ATP and Water. βE188 is an important active site residue that is believed to help extract a water molecule from ADP and P_i during the synthesis of ATP.[13] To better understand the structural aspect of the role that βE188 plays during the synthesis of ATP, we calculated the interatomic distances between the ε-oxygens of βE188 and that of all four oxygen atoms of P_i throughout the reaction coordinate. These data are recorded in Table S10 of the Supporting Information. (See Table S8 of the Supporting Information for conversion of model nomenclature to actual PDB nomenclature.)

In the half-closed state, the shortest distance from the ε-oxygen of βE188 to the nearest oxygen of the P_i analogue is just less than 10 Å (Table S10 of the Supporting Information). However, in the ADP- and P_i-bound state, the shortest distance from the ε-oxygen of βE188 to the nearest oxygen of the P_i analogue is 2.8 Å. This point further underscores the medial position of P_i in the P-loop binding pocket. In the transition state analogue, the γ-phosphate oxygen that is forming the leaving group water is nearly equidistant (3.8 Å) between the β-carbon of βA158 (Figure 7A) and the closest ε-oxygen of βE188 (Figure 8A and Animation S5 of the Supporting Information). In the product-bound state, the leaving group water remains in the proximity of an ε-oxygen of βE188, while it increases its distance from both ATP and the methyl group of βA158. These data strongly support our earlier proposals[32,35] regarding the mechanism of ATP synthesis, whereby βA158 maintains a position near the reaction center. Here, its hydrophobicity can be utilized in a concerted effort with βE188 to extract a water molecule from ADP and P_i, thus facilitating the formation of ATP.

Mg^{2+} Slides into a Tighter Coordination with a Nonbonding Oxygen of P_i during the Transition State and Even Tighter Coordination upon Formation of ATP. Previous fluorescence and EPR studies[64,65] were used to investigate the role of Mg^{2+} in the mechanism of F_1-ATPase by identifying the protein side chains that contribute to

dx.doi.org/10.1021/bi201595v | Biochemistry 2012, 51, 1532−1546

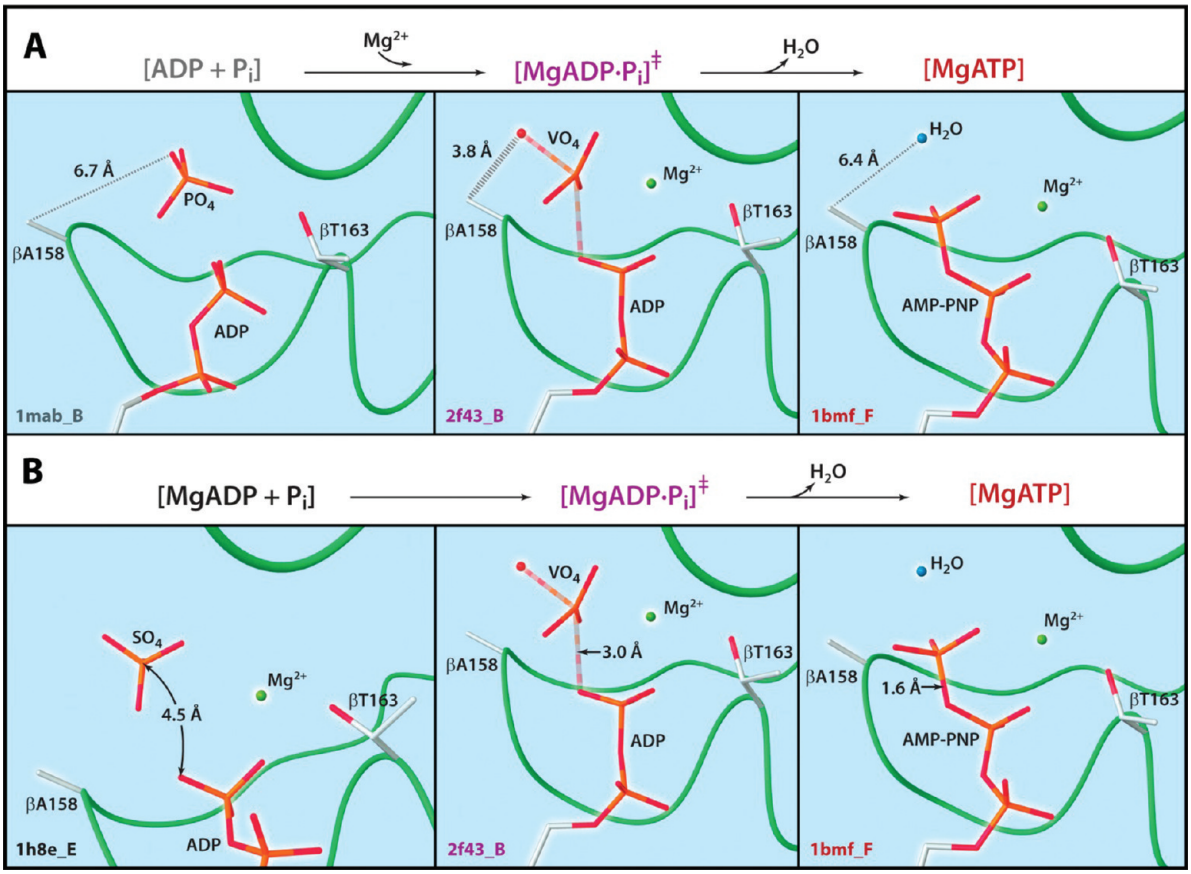

Figure 7. Positional dynamics of the active site P-loop clamp of the ATP synthase at the substrate level. (A) This illustration depicts changes in the positional relationship between the methyl group of βA158 and oxygen atoms of the γ-phosphate throughout the reaction coordinate. (B) This illustration depicts changes in the positional relationship of the proposed nucleophilic oxygen of the β-phosphate of ADP and the phosphorus atom of γ-phosphate throughout the reaction coordinate. All distances are reported in angstroms.

coordination of this metal and its relationship with nucleotide binding. The model proposed by Weber et al.[65] depicts the contacts of the first coordination sphere as consisting of three potential water molecules (not seen structurally as yet) in the active site, oxygen atoms from both the β- and γ-phosphates, and a hydroxyl group from the P-loop threonine of the β subunit. In the MgADP-F_1 complex, it has been reported that an undistorted first coordination sphere with purported waters would fit within the available space without interference from any side chain atoms.[65] However, in the MgATP-F_1 complex, there would be slight deformation of the first coordination sphere because of interference and overlap of active site side chains with the purported water molecules.[65] To better understand the structural changes in the positional relationship of Mg^{2+} within the active site, interatomic distances were calculated for the three nonaqueous contacts in the half-closed (1h8e_AE), transition state analogue (2f43_AB), and product-bound (1bmf_BF) states. These data are recorded in Table S11 of the Supporting Information.

When the half-closed state is observed, Mg^{2+} is within bonding length of both the hydroxyl group of βT163, and a nonbonding oxygen of ADP, and four water molecules form a nearly perfect octahedral coordination sphere with bond lengths of ~2.1 Å, as would be expected on the basis of the work of Guerger et al.[66] The P_i analogue (SO_4) is nearly 4.0 Å from Mg^{2+}, with one of the coordinating waters in the space between the analogue and the Mg^{2+}. However, upon formation of the transition state, Mg^{2+} appears to slide away from both βT163 and ADP while attaining a tighter configuration with the closest oxygen on V_i at 2.9 Å, resulting in distortion of the coordination sphere. In the work of Weber et al.,[67] Mg^{2+} was required for tight binding in the transition state complex to stabilize it. As ATP forms, Mg^{2+} continues its trend of tighter coordination with the nearest oxygen of the γ-phosphate by nearly 0.7 Å, but its interactions with the nearest oxygen of the β-phosphate and hydroxyl group of βT163 also become tighter, but to a lesser extent (<0.5 Å for each) (Figure 8B and Animation S6 of the Supporting Information). This trend in sequential binding modulation of Mg^{2+} within the active site from a loose to a tighter configuration was mentioned in the earlier work of Schuster and co-workers,[68,69] who studied metal−nucleotide interactions. While the octahedral coordination recovers somewhat from the transition state, it is still somewhat distorted when compared to the half-closed state. The data retrieved from this reaction model fit the expected paradigm of magnesium coordination outlined by Senior and co-workers.[65]

■ CONCLUSIONS

The novel visual comparative structural approach reported here has utilized currently available X-ray structural data[29,47−49] for the F_1 catalytic unit of ATP synthase to map out structural changes occurring at the active site during ATP synthesis. Interatomic distances between landmark atoms of both the peptide and the ligand were calculated to determine the nature of active site remodeling as well as changes in the positional

dx.doi.org/10.1021/bi201595v | Biochemistry 2012, 51, 1532−1546

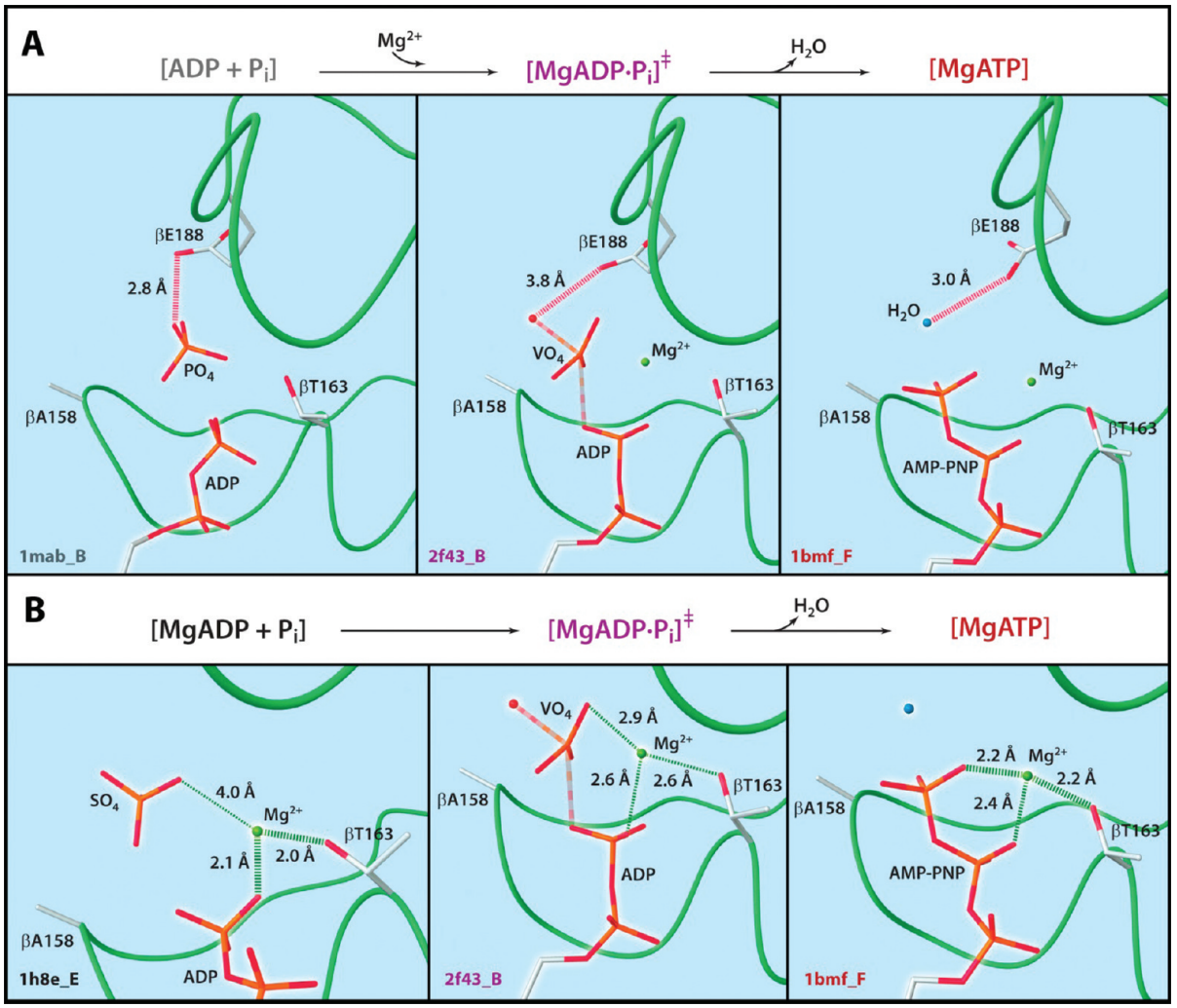

Figure 8. Positional dynamics of the active site P-loop clamp, at the substrate level. (A) This illustration depicts changes in the positional relationship between the carboxyl group of *β*E188 and oxygen atoms of the *γ*-phosphate throughout the reaction coordinate. (B) This illustration depicts changes in the positional relationship between Mg^{2+} and three coordinating atoms from the hydroxyl group of *β*T163 and oxygen atoms from both *β*- and *γ*-phosphates throughout the reaction coordinate. All distances are reported in angstroms.

relationships between the protein and ligand during ATP synthesis. With a spatial context of the interatomic relationships among the P-loop residues, Mg^{2+}, and P_i, comparison with a visual model of the reaction coordinate becomes a valuable tool for determining the more subtle changes that are not readily apparent by numeric value alone. As the active site undergoes the transitions from state to state, these key interactions change in a concerted manner (Table S12 of the Supporting Information). In a movie of reaction model 1 (also summarized in Figure 9 and Animation S7 of the Supporting Information), starting in the empty state, the P-loop clamp is closed while the active site clamp is stretched wide open relative to later intermediate steps in the reaction coordinate. In the next state with ADP and P_i bound to the active site, the P-loop clamp has since opened by 1.7 Å and the active site clamp has closed by >3 Å. In this ADP- and P_i-bound state, the *β*-phosphate of ADP is positioned closer to *β*T163 while P_i is positioned medially in the P-loop clamp. Upon binding of Mg^{2+} and formation of the transition state, the *β*-phosphate and P_i both move closer to *β*A158. Oxygen atoms from both *β*- and *γ*-phosphates participate in the first coordination sphere with Mg^{2+}, albeit in a distorted octahedron. These interactions create a spatial environment in which the oxygen leaving *γ*-phosphate is placed directly between the hydrophobic methyl group of *β*A158 and the carboxyl group of *β*E188 that plays a role in water extraction during ATP formation. In the final state following ATP formation, the P-loop clamp has maintained its position in relation to ATP, with the *γ*-phosphate staying in the proximity of the hydrophobic environment of *β*A158. The leaving group water moves out of the active site, away from *β*A158. With use of this visual reaction model, it becomes possible to see the concerted role of Mg^{2+} in both the placement and the orientation of P_i early in the reaction coordinate by sharing occupancy of the P-loop clamp. In the absence of Mg^{2+}, P_i does not assume the correct position in the active site next to *β*A158, and therefore, several important interactions in the active site are disrupted.

Using this novel visual comparative structural approach to study the conformational changes in the active site of an enzyme through the reaction coordinate offers a valuable perspective into enzyme mechanism that is difficult to achieve with interatomic distances alone. By mapping landmark residues in the active site to create a triangulated map of positional changes, we are able to isolate conformational

dx.doi.org/10.1021/bi201595v | *Biochemistry* 2012, 51, 1532–1546

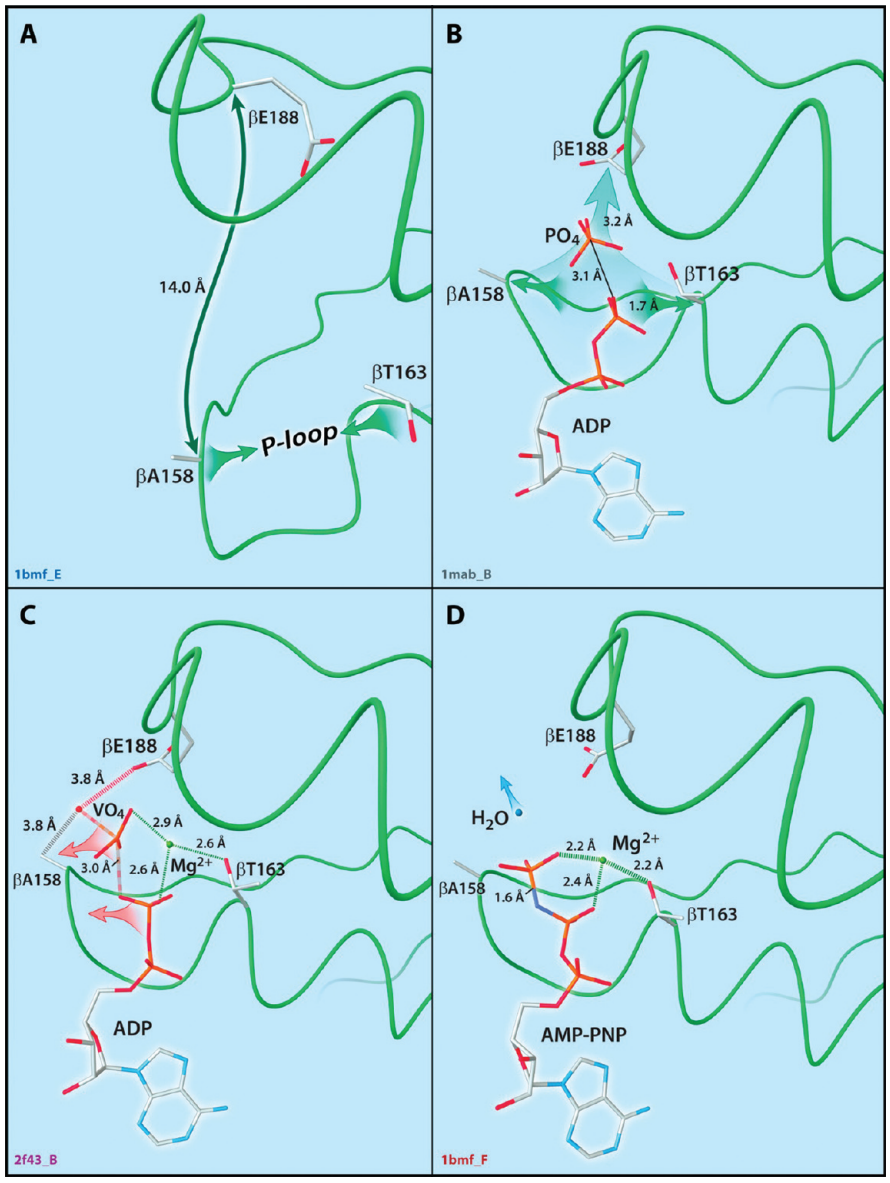

Figure 9. Diagram illustrating the pivotal role that Mg^{2+} may play in the proper positioning and orientation of P_i in the active site adjacent to *β*A158. (A) This step depicts the empty state of the enzyme in which the active site clamp is open to nearly 14.0 Å, while the P-loop clamp is in a closed state. (B) This step illustrates the closing of the active site clamp by 3.2 Å and an opening of the P-loop clamp by 1.7 Å. P_i is positioned medially in the active site cleft, nearly equidistant from both *β*A158 and *β*T163 in the absence of Mg^{2+}. (C) This step illustrates the effects of Mg^{2+} binding whereby both the P_i and the *β*-phosphate of ADP move closer to *β*A158. Formation of the transition state places the oxygen leaving group between the hydrophobic methyl group of *β*A158 and the carboxyl group of *β*E188, which aids both in water formation and in its subsequent removal from newly formed ATP. (D) This step illustrates the formation of ATP and removal of the leaving group water. All distances are reported in angstroms.

changes to a given context, in this case, to the purported axis of *γ* subunit rotation. This feature is valuable for deciphering specific and complex concerted three-dimensional interrelations between key side chains and the bound ligand, which help visualize changes in both position and orientation. In summary, this novel visual comparative structural methodology gives the viewer an improved structural understanding of the mechanism and provides insight into future studies. Animation and interpolation studies have been used and developed extensively in past projects,[70−72] but this is the first study to tackle the motor components of an enzyme that uses rotational elements in its mechanism.

Using structural data to elucidate a given enzymatic mechanism has many potential pitfalls. While all PDB structures used in this study have a resolution of 2.0−3.0 Å, improved structures at even greater resolution would significantly increase the level of confidence of our results. However, the use of a crystallographic structure is a compromise in that it is not a true representation of a solution structure, especially upon analysis of the minute changes in interatomic distances later in the reaction coordinate. In terms of the average normalized temperature factor (Table S13 and Figure S1 of the Supporting Information), most of the regions in this study were below average per their respective PDB files, with the exception of the P-loop regions of 1mab_B, 2f43_b, and 1bmf_E. The final results are a product of the data used, so vast improvements in results could be attained with structures that have greater resolution and lower temperature factors, although this may be difficult to achieve. In fact, examination of the recent ground state structure of the bovine mitochondrial

dx.doi.org/10.1021/bi201595v | *Biochemistry* 2012, 51, 1532−1546

F_1-ATPase at 1.95 Å[73] demonstrates a high degree of similarity to the interatomic distances of the empty and product-bound states used in our model. While Dittrich et al.[74] have performed quantum mechanics/molecular mechanics (QM/MM) simulations on F_1-ATPase in the study of the mechanism of ATP hydrolysis, their work focused more on the roles of βK162, βE188, and βR189 in hydrolysis. Future studies using QM/MM simulations might complement our results by providing a balance between interpolation and simulated dynamics when utilizing conformational intermediates of biological systems.

■ ASSOCIATED CONTENT

Supporting Information

Tables S1−S13, Figure S1, Animations S1−S7, and supplemental text. This material is available free of charge via the Internet at http://pubs.acs.org.

■ AUTHOR INFORMATION

Corresponding Author

*Telephone: (410) 955-3827. Fax: (410) 614-1944. E-mail: ppederse@jhmi.edu.

Funding

This study was supported by National Institutes of Health Grant CA 10951 to P.L.P.

■ ACKNOWLEDGMENTS

We thank Dr. Lee G. Pedersen, a theoretical and computational chemist and Professor in the Department of Chemistry of the University of North Carolina (Chapel Hill, NC), Dr. Jonathan Pevsner, Associate Professor in the Department of Neuroscience with expertise in Bioinformatics at The Johns Hopkins University School of Medicine, and Dr. Jason C. Mussell, Assistant Professor in the Department of Cell Biology and Anatomy at Louisiana State University School of Medicine (New Orleans, LA), for their review, valuable comments, and suggestions regarding an earlier version of the manuscript. We also thank a former co-worker, Dr. Chen Chen, now a structural biologist and Research Associate at the Center for Advanced Technology (CARB), for his assistance and insightful recommendations.

■ ABBREVIATIONS

PDB, Protein Data Bank; EM, electron microscopy; V_i, orthovanadate; P_i, inorganic phosphate; MgAMP-PNP, magnesium-5′-adenylyl imidodiphosphate; EPR, electron paramagnetic resonance; QM/MM, quantum mechanics/molecular mechanics.

■ REFERENCES

(1) Catterall, W. A., Coty, W. A., and Pedersen, P. L. (1973) Adenosine triphosphatase from rat liver mitochondria. 3. Subunit composition. *J. Biol. Chem. 248*, 7427−7431.

(2) Catterall, W. A., and Pedersen, P. L. (1971) Adenosine triphosphatase from rat liver mitochondria. I. Purification, homogeneity, and physical properties. *J. Biol. Chem. 246*, 4987−4994.

(3) Catterall, W. A., and Pedersen, P. L. (1974) Structural and Catalytic Properties of Mitochondrial Adenosine Triphosphatase. *Biochem. Soc. Spec. Publ. 4*, 63−88.

(4) al-Shawi, M. K., and Senior, A. E. (1992) Catalytic sites of *Escherichia coli* F_1-ATPase. Characterization of unisite catalysis at varied pH. *Biochemistry 31*, 878−885.

(5) Al-Shawi, M. K., and Senior, A. E. (1988) Complete kinetic and thermodynamic characterization of the unisite catalytic pathway of *Escherichia coli* F_1-ATPase. Comparison with mitochondrial F_1-ATPase and application to the study of mutant enzymes. *J. Biol. Chem. 263*, 19640−19648.

(6) Weber, J., Bijol, V., Wilke-Mounts, S., and Senior, A. E. (2002) Cysteine-reactive fluorescence probes of catalytic sites of ATP synthase. *Arch. Biochem. Biophys. 397*, 1−10.

(7) Weber, J., and Senior, A. E. (2000) Features of F_1-ATPase catalytic and noncatalytic sites revealed by fluorescence lifetimes and acrylamide quenching of specifically inserted tryptophan residues. *Biochemistry 39*, 5287−5294.

(8) al-Shawi, M. K., Parsonage, D., and Senior, A. E. (1989) Kinetic characterization of the unisite catalytic pathway of seven β-subunit mutant F_1-ATPases from *Escherichia coli*. *J. Biol. Chem. 264*, 15376−15383.

(9) Weber, J., Bowman, C., and Senior, A. E. (1996) Specific tryptophan substitution in catalytic sites of *Escherichia coli* F_1-ATPase allows differentiation between bound substrate ATP and product ADP in steady-state catalysis. *J. Biol. Chem. 271*, 18711−18718.

(10) Boyer, P. (1989) A perspective of the binding change mechanism for ATP synthesis. *FASEB J. 3*, 2164−2178.

(11) Capaldi, R. A., Schulenberg, B., Murray, J., and Aggeler, R. (2000) Cross-linking and electron microscopy studies of the structure and functioning of the *Escherichia coli* ATP synthase. *J. Exp. Biol. 203*, 29−33.

(12) Duncan, T. M., Bulygin, V. V., Zhou, Y., Hutcheon, M. L., and Cross, R. L. (1995) Rotation of subunits during catalysis by *Escherichia coli* F_1-ATPase. *Proc. Natl. Acad. Sci. U.S.A. 92*, 10964−10968.

(13) Pedersen, P. L., Ko, Y. H., and Hong, S. (2000) ATP synthases in the year 2000: Defining the different levels of mechanism and getting a grip on each. *J. Bioenerg. Biomembr. 32*, 423−432.

(14) Noji, H., Yasuda, R., Yoshida, M., and Kinosita, K. (1997) Direct observation of the rotation of F_1-ATPase. *Nature 386*, 299−302.

(15) Omote, H., Sambonmatsu, N., Saito, K., Sambongi, Y., Iwamoto-Kihara, A., Yanagida, T., Wada, Y., and Futai, M. (1999) The γ-subunit rotation and torque generation in F_1-ATPase from wild-type or uncoupled mutant *Escherichia coli*. *Proc. Natl. Acad. Sci. U.S.A. 96*, 7780−7784.

(16) Hong, S., and Pedersen, P. L. (2003) ATP synthases: Insights into their motor functions from sequence and structural analyses. *J. Bioenerg. Biomembr. 35*, 95−120.

(17) Saraste, M., Sibbald, P. R., and Wittinghofer, A. (1990) The P-loop: A common motif in ATP- and GTP-binding proteins. *Trends Biochem. Sci. 15*, 430−434.

(18) Williams, N., Hullihen, J., and Pedersen, P. L. (1988) Mitochondrial ATP synthase: Role of metal binding in structure and function. *Prog. Clin. Biol. Res. 273*, 87−92.

(19) Weber, J., and Senior, A. E. (1997) Catalytic mechanism of F_1-ATPase. *Biochim. Biophys. Acta 1319*, 19−58.

(20) Futai, M., Park, M., Iwamoto, A., Omote, H., and Maeda, M. (1994) Catalysis and energy coupling of H^+-ATPase (ATP synthase): Molecular biological approaches. *Biochim. Biophys. Acta 1187*, 165−170.

(21) Hsu, S. Y., Noumi, T., Takeyama, M., Maeda, M., Ishibashi, S., and Futai, M. (1987) β-subunit of *Escherichia coli* F_1-ATPase. An amino acid replacement within a conserved sequence (G-X-X-X-X-G-K-T/S) of nucleotide-binding proteins. *FEBS Lett. 218*, 222−226.

(22) Iwamoto, A., Park, M. Y., Maeda, M., and Futai, M. (1993) Domains near ATP γ phosphate in the catalytic site of H^+-ATPase. Model proposed from mutagenesis and inhibitor studies. *J. Biol. Chem. 268*, 3156−3160.

(23) Omote, H., Le, N. P., Park, M. Y., Maeda, M., and Futai, M. (1995) β subunit Glu-185 of *Escherichia coli* H^+-ATPase (ATP synthase) is an essential residue for cooperative catalysis. *J. Biol. Chem. 270*, 25656−25660.

(24) Park, M. Y., Omote, H., Maeda, M., and Futai, M. (1994) Conserved Glu-181 and Arg-182 residues of *Escherichia coli* H^+-ATPase (ATP synthase) β subunit are essential for catalysis: Properties of 33 mutants between βGlu-161 and βLys-201 residues. *J. Biochem. 116*, 1139−1145.

(25) Takeyama, M., Ihara, K., Moriyama, Y., Noumi, T., Ida, K., Tomioka, N., Itai, A., Maeda, M., and Futai, M. (1990) The glycine-rich sequence of the β subunit of *Escherichia coli* H^+-ATPase is important for activity. *J. Biol. Chem. 265*, 21279−21284.
(26) Parsonage, D., Wilke-Mounts, S., and Senior, A. E. (1988) *E. coli* F_1-ATPase: site-directed mutagenesis of the β-subunit. *FEBS Lett. 232*, 111−114.
(27) Parsonage, D., Al-Shawi, M. K., and Senior, A. E. (1988) Directed mutations of the strongly conserved lysine 155 in the catalytic nucleotide-binding domain of β-subunit of F_1-ATPase from *Escherichia coli*. *J. Biol. Chem. 263*, 4740−4744.
(28) al-Shawi, M. K., Parsonage, D., and Senior, A. E. (1990) Thermodynamic analyses of the catalytic pathway of F_1-ATPase from *Escherichia coli*. Implications regarding the nature of energy coupling by F_1-ATPases. *J. Biol. Chem. 265*, 4402−4410.
(29) Chen, C., Saxena, A. K., Simcoke, W. N., Garboczi, D. N., Pedersen, P. L., and Ko, Y. H. (2006) Mitochondrial ATP synthase. Crystal structure of the catalytic F_1 unit in a vanadate-induced transition-like state and implications for mechanism. *J. Biol. Chem. 281*, 13777−13783.
(30) Smith, C. A., and Rayment, I. (1996) X-ray structure of the magnesium(II)·ADP·vanadate complex of the *Dictyostelium discoideum* myosin motor domain to 1.9 Å resolution. *Biochemistry 35*, 5404−5417.
(31) Fisher, A. J., Smith, C. A., Thoden, J. B., Smith, R., Sutoh, K., Holden, H. M., and Rayment, I. (1995) X-ray structures of the myosin motor domain of *Dictyostelium discoideum* complexed with MgADP·BeF_x and MgADP·AlF_4^-. *Biochemistry 34*, 8960−8972.
(32) Ko, Y. H., Bianchet, M., Amzel, L. M., and Pedersen, P. L. (1997) Novel insights into the chemical mechanism of ATP synthase. Evidence that in the transition state the γ-phosphate of ATP is near the conserved alanine within the P-loop of the β-subunit. *J. Biol. Chem. 272*, 18875−18881.
(33) Cremo, C. R., Loo, J. A., Edmonds, C. G., and Hatlelid, K. M. (1992) Vanadate catalyzes photocleavage of adenylate kinase at proline-17 in the phosphate-binding loop. *Biochemistry 31*, 491−497.
(34) Frye, J. J., Klenchin, V. A., Bagshaw, C. R., and Rayment, I. (2010) Insights into the importance of hydrogen bonding in the γ-phosphate binding pocket of myosin: Structural and functional studies of serine 236. *Biochemistry 49*, 4897−4907.
(35) Ko, Y. H., Hong, S., and Pedersen, P. L. (1999) Chemical mechanism of ATP synthase. Magnesium plays a pivotal role in formation of the transition state where ATP is synthesized from ADP and inorganic phosphate. *J. Biol. Chem. 274*, 28853−28856.
(36) Löbau, S., Weber, J., and Senior, A. E. (1998) Catalytic site nucleotide binding and hydrolysis in F_1F_0-ATP synthase. *Biochemistry 37*, 10846−10853.
(37) Ahmad, Z., and Senior, A. E. (2004) Mutagenesis of residue βArg-246 in the phosphate-binding subdomain of catalytic sites of *Escherichia coli* F_1-ATPase. *J. Biol. Chem. 279*, 31505−31513.
(38) Senior, A. E., Weber, J., and Nadanaciva, S. (2000) The catalytic transition state in ATP synthase. *J. Bioenerg. Biomembr. 32*, 523−529.
(39) Ahmad, Z., and Senior, A. E. (2005) Identification of phosphate binding residues of *Escherichia coli* ATP synthase. *J. Bioenerg. Biomembr. 37*, 437−440.
(40) Ahmad, Z., and Senior, A. E. (2004) Role of βAsn-243 in the phosphate-binding subdomain of catalytic sites of *Escherichia coli* F_1-ATPase. *J. Biol. Chem. 279*, 46057−46064.
(41) Ahmad, Z., and Senior, A. E. (2005) Modulation of charge in the phosphate binding site of *Escherichia coli* ATP synthase. *J. Biol. Chem. 280*, 27981−27989.
(42) Ahmad, Z., and Senior, A. E. (2005) Involvement of ATP synthase residues αArg-376, βArg-182, and βLys-155 in P_i binding. *FEBS Lett. 579*, 523−528.
(43) Löbau, S., Weber, J., Wilke-Mounts, S., and Senior, A. E. (1997) F_1-ATPase, roles of three catalytic site residues. *J. Biol. Chem. 272*, 3648−3656.
(44) Nadanaciva, S., Weber, J., and Senior, A. E. (1999) The role of β-Arg-182, an essential catalytic site residue in *Escherichia coli* F_1-ATPase. *Biochemistry 38*, 7670−7677.
(45) Senior, A. E., Nadanaciva, S., and Weber, J. (2000) Rate acceleration of ATP hydrolysis by F_1F_o-ATP synthase. *J. Exp. Biol. 203*, 35−40.
(46) Senior, A. E., Nadanaciva, S., and Weber, J. (2002) The molecular mechanism of ATP synthesis by F_1F_0-ATP synthase. *Biochim. Biophys. Acta 1553*, 188−211.
(47) Abrahams, J. P., Leslie, A. G., Lutter, R., and Walker, J. E. (1994) Structure at 2.8 Å resolution of F_1-ATPase from bovine heart mitochondria. *Nature 370*, 621−628.
(48) Bianchet, M. A., Hullihen, J., Pedersen, P. L., and Amzel, L. M. (1998) The 2.8-Å structure of rat liver F_1-ATPase: Configuration of a critical intermediate in ATP synthesis/hydrolysis. *Proc. Natl. Acad. Sci. U.S.A. 95*, 11065−11070.
(49) Menz, R. I., Walker, J. E., and Leslie, A. G. (2001) Structure of bovine mitochondrial F_1-ATPase with nucleotide bound to all three catalytic sites: Implications for the mechanism of rotary catalysis. *Cell 106*, 331−341.
(50) Altschul, S. F., Madden, T. L., Schäffer, A. A., Zhang, J., Zhang, Z., Miller, W., and Lipman, D. J. (1997) Gapped BLAST and PSI-BLAST: A new generation of protein database search programs. *Nucleic Acids Res. 25*, 3389−3402.
(51) Gledhill, J. R., Montgomery, M. G., Leslie, A. G. W., and Walker, J. E. (2007) How the regulatory protein, IF_1, inhibits F_1-ATPase from bovine mitochondria. *Proc. Natl. Acad. Sci. U.S.A. 104*, 15671−15676.
(52) Gledhill, J. R., Montgomery, M. G., Leslie, A. G. W., and Walker, J. E. (2007) Mechanism of inhibition of bovine F_1-ATPase by resveratrol and related polyphenols. *Proc. Natl. Acad. Sci. U.S.A. 104*, 13632−13637.
(53) Bowler, M. W., Montgomery, M. G., Leslie, A. G. W., and Walker, J. E. (2006) How azide inhibits ATP hydrolysis by the F-ATPases. *Proc. Natl. Acad. Sci. U.S.A. 103*, 8646−8649.
(54) Watt, I. N., Montgomery, M. G., Runswick, M. J., Leslie, A. G. W., and Walker, J. E. (2010) Bioenergetic cost of making an adenosine triphosphate molecule in animal mitochondria. *Proc. Natl. Acad. Sci. U.S.A. 107*, 16823−16827.
(55) Sanchez-Weatherby, J., Bowler, M. W., Huet, J., Gobbo, A., Felisaz, F., Lavault, B., Moya, R., Kadlec, J., Ravelli, R. B. G., and Cipriani, F. (2009) Improving diffraction by humidity control: A novel device compatible with X-ray beamlines. *Acta Crystallogr. D65*, 1237−1246.
(56) Berman, H. M., Battistuz, T., Bhat, T. N., Bluhm, W. F., Bourne, P. E., Burkhardt, K., Feng, Z., Gilliland, G. L., Iype, L., Jain, S., Fagan, P., Marvin, J., Padilla, D., Ravichandran, V., Schneider, B., Thanki, N., Weissig, H., Westbrook, J. D., and Zardecki, C. (2002) The Protein Data Bank. *Acta Crystallogr. D58*, 899−907.
(57) Schwede, T., Kopp, J., Guex, N., and Peitsch, M. C. (2003) SWISS-MODEL: An automated protein homology-modeling server. *Nucleic Acids Res. 31*, 3381−3385.
(58) DeLano, W. L. (2002) *The PyMOL Molecular Graphics System*, DeLano Scientific, San Carlos, CA.
(59) Carugo, O., and Argos, P. (1997) Correlation between side chain mobility and conformation in protein structures. *Protein Eng. 10*, 777−787.
(60) Braig, K., Menz, R. I., Montgomery, M. G., Leslie, A. G., and Walker, J. E. (2000) Structure of bovine mitochondrial F_1-ATPase inhibited by Mg^{2+}ADP and aluminium fluoride. *Structure 8*, 567−573.
(61) Watanabe, R., Iino, R., and Noji, H. (2010) Phosphate release in F_1-ATPase catalytic cycle follows ADP release. *Nat. Chem. Biol. 6*, 814−820.
(62) Manimekalai, M. S. S., Kumar, A., Jeyakanthan, J., and Grüber, G. (2011) The transition-like state and P_i entrance into the catalytic a subunit of the biological engine A-ATP synthase. *J. Mol. Biol. 408*, 736−754.
(63) Mildvan, A. S. (1997) Mechanisms of signaling and related enzymes. *Proteins 29*, 401−416.

(64) Frasch, W. D. (2000) The participation of metals in the mechanism of the F_1-ATPase. *Biochim. Biophys. Acta 1458*, 310−325.
(65) Weber, J., Hammond, S. T., Wilke-Mounts, S., and Senior, A. E. (1998) Mg^{2+} coordination in catalytic sites of F_1-ATPase. *Biochemistry 37*, 608−614.
(66) Guerger, M. J., MacGillavry, C. H., Henry, N. F. M., Lonsdale, K., and Rieck, G. D. (1968) *Int. Tables X-ray Crystallogr.,*, 257−269.
(67) Weber, J., and Senior, A. E. (2000) ATP synthase: What we know about ATP hydrolysis and what we do not know about ATP synthesis. *Biochim. Biophys. Acta 1458*, 300−309.
(68) Gruys, K. J., Urbauer, J. L., and Schuster, S. M. (1985) Metal-nucleotide structural characteristics during catalysis by beef heart mitochondrial F_1. *J. Biol. Chem. 260*, 6533−6540.
(69) Daggett, S. G., Gruys, K. J., and Schuster, S. M. (1985) Metal interactions with beef heart mitochondrial ATPase. *J. Biol. Chem. 260*, 6213−6218.
(70) Booth, A. G. (2001) Visualizing protein conformational changes on a personal computer: α carbon pseudo bonding as a constraint for interpolation in internal coordinate space. *J. Mol. Graphics Modell. 19*, 481−486.
(71) Stroud, R. M., and Finer-Moore, J. S. (2003) Conformational dynamics along an enzymatic reaction pathway: Thymidylate synthase, "the movie". *Biochemistry 42*, 239−247.
(72) Zeev-Ben-Mordehai, T., Silman, I., and Sussman, J. L. (2003) Acetylcholinesterase in motion: Visualizing conformational changes in crystal structures by a morphing procedure. *Biopolymers 68*, 395−406.
(73) Bowler, M. W., Montgomery, M. G., Leslie, A. G. W., and Walker, J. E. (2007) Ground state structure of F_1-ATPase from bovine heart mitochondria at 1.9 Å resolution. *J. Biol. Chem. 282*, 14238−14242.
(74) Dittrich, M., Hayashi, S., and Schulten, K. (2003) On the mechanism of ATP hydrolysis in F_1-ATPase. *Biophys. J. 85*, 2253−2266.
(75) Schobert, B. (1998) Do ATP^{4-} and Mg^{2+} bind stepwise to the F_1-ATPase of *Halobacterium saccharovorum*? *Eur. J. Biochem. 254*, 363−370.